JACS
JOURNAL OF THE AMERICAN CHEMICAL SOCIETY
Article
pubs.acs.org/JACS

Structural Insights into the Ferroxidase Site of Ferritins from Higher Eukaryotes

Ivano Bertini,*[,†,‡] Daniela Lalli,[†] Stefano Mangani,[†,§] Cecilia Pozzi,[§] Camilla Rosa,[†] Elizabeth C. Theil,[∥,⊥] and Paola Turano[†,‡]

[†]Magnetic Resonance Center (CERM) and [‡]Department of Chemistry, University of Florence, 50019 Sesto Fiorentino, Florence, Italy

[§]Department of Chemistry, University of Siena, 53100 Siena, Italy

[∥]Council on BioIron at Children's Hospital Oakland Research Institute, Oakland, California 94609, United States

[⊥]Department of Nutritional Sciences and Toxicology, University of California, Berkeley, California 94720, United States

Supporting Information

ABSTRACT: The first step of iron biomineralization mediated by ferritin is the oxidation at the ferroxidase active site of two ferrous ions to a diferric oxo/hydroxo species. Metal-loaded ferritin crystals obtained by soaking crystals of frog ferritin in $FeSO_4$ and $CuSO_4$ solutions followed by flash freezing provided X-ray crystal structures of the tripositive iron and bipositive copper adducts at 2.7 and 2.8 Å resolution, respectively. At variance with the already available structures, the crystal form used in this study contains 24 independent subunits in the asymmetric unit permitting comparison between them. For the first time, the diferric species at the ferroxidase site is identified in ferritins from higher eukaryotes. Anomalous difference Fourier maps for crystals (iron crystal 1) obtained after long soaking times in $FeSO_4$ solution invariantly showed diferric species with a Fe−Fe average distance of 3.1 ± 0.1 Å, strongly indicative of the presence of a μ-oxo/hydroxo bridge between the irons; protein ligands for each iron ion (Fe1 and Fe2) were also unequivocally identified and found to be the same in all subunits. For copper bound ferritin, dicopper(II) centers are also observed. While copper at site 1 is essentially in the same position and has the same coordination environment as Fe1, copper at site 2 is displaced toward His54, now acting as a ligand; this results in an increased intermetal distance (4.3 ± 0.4 Å). His54 coordination and longer metal−metal distances might represent peculiar features of divalent cations at the ferroxidase site. This oxidation-dependent structural information may provide key features for the mechanistic pathway in ferritins from higher eukaryotes that drive uptake of bivalent cation and release of ferric products at the catalytic site. This mechanism is supported by the X-ray picture obtained after only 1 min of soaking in $FeSO_4$ solutions (iron crystal 2) which reasonably contain the metal at different oxidation states. Here two different di-iron species are trapped in the active site, with intermetal distances corresponding to those of the ferric dimer in crystal 1 and of the dicopper centers and corresponding rearrangement of the His54 side chain.

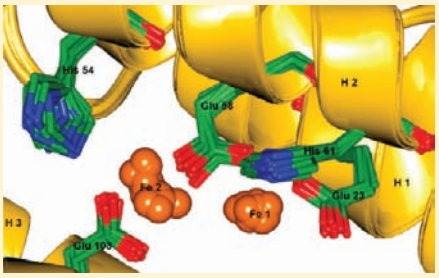

INTRODUCTION

Ferritins are intracellular proteins capable of storing thousands of iron(III) ions as a solid mineral.[1] The ferritin molecule is a multimeric system formed by 24 subunits that assemble in such a way to form an external cage around the biomineral storage cavity (Figure 1).[2] The subunits are characterized by a four-helix bundle structure. Iron(II) enters the protein shell through ion channels and reaches the active site, known as the ferroxidase site, constituted by a dinuclear metal ion binding site. Here, the two substrates, iron(II) and O_2, are coupled to obtain iron(III) mineral precursors.[2−5] The ferroxidase site functions as a gated site for the transfer of ferric products into the cavity following oxidation.[6,7] Here a structural characterization is reported for frog ferritin, a particular system constituted by 24 identical subunits, called M subunits, and compared with the already available structural information on similar systems.

Studying iron in ferritins is difficult because of the transient nature of the metal binding at this low-affinity site (K_d of the order of 10^{-5} M),[8] which has prevented up to now a full understanding of the iron binding by X-ray crystallography. Most of the structural information about iron-binding has been inferred either from spectroscopy[9] or through metal substitution.[2−4] X-ray crystal structures of iron-bound ferritins available for some organisms reflect the transient nature of iron−protein interactions.

In anaerobes, ferritin has been proposed to protect the organisms from traces of oxygen and its partially reduced derivatives.[10] The structure of ferritin from the anaerobe *Pyrococcus furiosus*[11] is paradigmatic, with three iron ions detected under aerobic conditions (Figure S1, Supporting Information): an iron site A appears to be the highest affinity

Received: October 26, 2011
Published: March 18, 2012

dx.doi.org/10.1021/ja210084n | J. Am. Chem. Soc. 2012, 134, 6169−6176

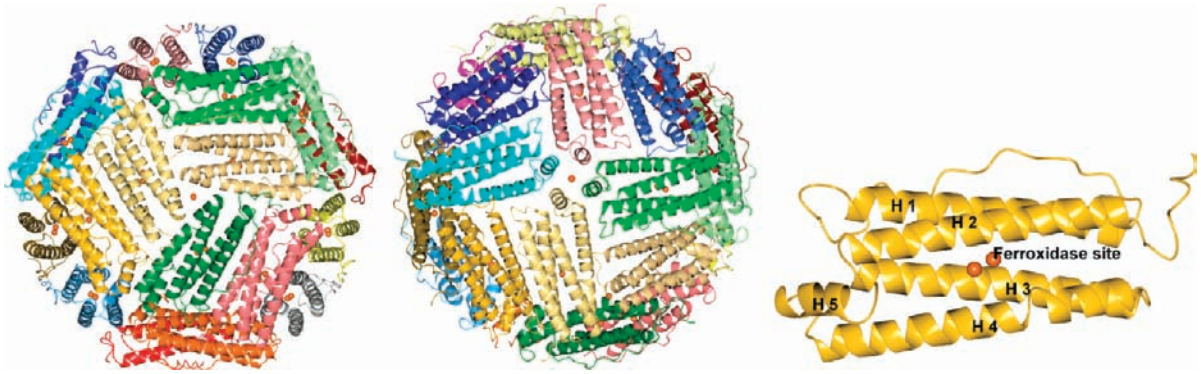

Figure 1. Two different views of the nanocage structure of ferritin obtained for Fe crystal 2: (a) centered on the C3 pore and (b) centered on the C4 pore. In (c), the structure of a single four-helix bundle subunit is shown together with helix numbering. In all panels, orange spheres represent iron atoms.

site since it is found occupied in the isolated protein, while sites B and C are found occupied only after soaking under aerobic conditions. The closest iron−iron distances have been found between sites A and B and vary between 2.6 and 3.6 Å in the different subunits. Among eukaryotic proteins, iron has been observed only at the ferroxidase site of marine pennate diatoms *Pseudonitzschia multiseries*.[12] This ferritin is largely divergent from those of other eukaryotes. A putative iron site similar to the A site of *P. furiosus* is found occupied by a water molecule (Figure S1, Supporting Information). An iron atom is observed bound to four glutamate residues in a site that is close, but not coincident, with site B of *P. furiosus*. Two other iron ions are positioned toward the protein core; neither of them corresponds to site C of *P. furiosus*. This variability of binding sites possibly reflects the transient iron binding and gives the perception that further efforts are needed to attempt an understanding of the system.

No iron-bound crystal structure is available for ferritin from higher eukaryotes. The only structural data available on the ferroxidase site have been obtained from X-ray absorption spectroscopy on the present system.[9] In that study, three different states have been trapped by rapid freeze quench of iron(II) ferritin reacting with O_2.[9] An initial diferrous, high-spin state is described with iron being in an average six-coordinated environment with a Fe−Fe distance of 3.44 Å. After 25 ms, a peroxodiferric intermediate has been described with the very short Fe−Fe distance of 2.53 Å, which rapidly (in about 1 min) evolves toward a diferric μ-oxo/hydroxo species with a Fe−Fe distance of 3.00 Å.[9]

A better characterization of the iron site is available for the ferritin-like proteins called bacterioferritins. They are 24-mer oligomeric proteins containing both binuclear iron centers and b-type hemes. Their primary functions have been proposed to be detoxification of iron or protection against O_2 and its radical products.[13] At variance with ferritins, it is generally accepted that in bacterioferritins, the iron at the catalytic center is stably bound,[2,14] acts as a cofactor, and displays an enzymatic role in the mineralization process.[2,14] As a consequence of this stability, dinuclear iron clusters have been more easily observed by X-ray crystallography at the catalytic site of bacterioferritins. The di-iron species obtained by soaking (<15 min) apobacterionferritin crystals in iron(II) solutions under aerobic conditions, followed by flash freezing, was proposed to be in the reduced state. The structure of the metal center has a symmetric architecture, with one His and one Glu residue per iron and two bridging Glu residues.[14,15] The metal−metal distance is about 4 Å in *Pseudomonas aeruginosa* bacterioferritin[15] and 3.7 Å in *Escherichia coli* bacterioferritin.[14] In the latter system, longer soaking times provided a metal center proposed to be a μ-oxo/hydroxo di-iron(III) species, with an intact coordination sphere as far as the protein residues are concerned[14] and an intermetal distance of 3.6 Å, which is similar to that of other di-iron enzymes.[11,12,16−19] In *P. aeruginosa* bacterioferritin the ferroxidase site was found devoid of iron upon oxidation.[15]

We report here crystal structures of iron-loaded frog M ferritin determined by flash freezing crystals soaked for different times in iron(II) solutions under aerobic conditions. These structures provide the first X-ray picture of iron(III) products at the ferroxidase site in higher eukaryotes ferritins.

With very short soaking times (1 min), two different iron-protein binding modes at the catalytic site have been obtained. With the same approach, the structure of the copper(II)-bound form has been solved, which may represent a model for the short-lived iron(II)-ferritin, i.e., the reactant species.

All together these structures provide a picture of the mechanism for the reaction at the ferroxidase site: here, iron oxidation by dioxygen is accompanied by a decrease in the intermetal distance and in the number of protein residues involved in metal coordination that facilitate release of the products as di-iron clusters.

EXPERIMENTAL PROCEDURES

Crystallization. Frog M ferritin was expressed and purified as previously described.[3] Crystals suitable for X-ray crystallography were grown using different procedures. One type of Fe-ferritin crystal (Fe crystal 1) was prepared from an iron preloaded protein solution using the sitting drop vapor diffusion technique at 20 °C. Iron loading was performed in aerobic conditions by adding a freshly prepared aqueous solution of $FeSO_4{\cdot}7H_2O$ to a 14 mg/mL demineralized ferritin solution in 20 mM TrisHCl at pH 7.5, in the approximate ratio of 2 irons/subunit. Drops were prepared by mixing equal volumes (2 μL) of iron-loaded ferritin solution and a precipitant solution of 2 M sodium formate. Crystals of the iron-loaded frog M ferritin grew in 4−7 days as rust-orange prisms. Further iron loading of the crystals was done by adding 1 μL of a freshly prepared 60 mM $FeSO_4{\cdot}7H_2O$ solution to the crystallization drop (iron concentration into the drop: ≈ 10 mM or stoichiometric ratio: ≈ 45 irons/subunit). After 90 min from the iron addition, the crystals were transferred to a cryoprotectant solution (made of 20% ethylene glycol and 80% precipitant solution) and flash frozen in liquid nitrogen.

A second type of iron-loaded crystal (Fe crystal 2) was obtained from demineralized frog M ferritin (14 mg/mL solution in 20 mM TrisHCl at pH 7.5) using 2.1 M sodium formate as precipitant in a

sitting drop setup (drops made of 4 μL protein +2 μL precipitant). One μL of a 64 mM $FeSO_4 \cdot 7H_2O$ solution was added to the 6 μL drop containing the demineralized crystal, obtaining an approximate Fe/subunit ratio of 24. After 1 min, the crystal (Fe crystal 2) was fished in a cryoloop, transferred to the cryosolution (see above), and frozen in liquid nitrogen. At the moment of freezing, the crystal had a much paler orange color with respect to Fe crystal 1.

The copper-loaded crystals were prepared by crystallizing a 7 mg/mL demineralized ferritin solution in 20 mM TrisHCl at pH 7.5 with 2.5 M sodium formate as precipitant in the same crystallization setup as the iron-loaded ferritin. Drops were prepared by mixing 4 μL of the above protein solution and 2 μL of precipitant. The drops containing the demineralized ferritin crystals were then treated with 1 μL of a 20 mM $CuSO_4 \cdot 5H_2O$ solution (approximate Cu/subunit ratio of 16). After 24 h the crystals have been transferred to a cryoprotectant solution (made of 20% ethylene glycol and 80% 3 M sodium formate) and flash frozen in liquid nitrogen.

Data Collection, Structure Solution, and Refinement. Data collection and refinement statistics for the three structures are reported in Table S1, Supporting Information.

A complete anomalous data set of the iron-loaded frog M ferritin was collected from crystal type 1 at the European Synchrotron Radiation Facility, Grenoble, France (ESRF) on beamline ID14-4 at the Zn−K edge (λ = 1.2915 Å, the longest available wavelength on that beamline). Images were collected at 100 K on the charge-coupled device detector Area Detector Systems Corporation Quantum Q315r. The data were integrated using the program MOSFLM 7.0.4[20] and scaled with SCALA[21] from the CCP4 suite.[22] Fe crystal 1 belonged to the trigonal space group $P3_121$ with cell parameters a = 210.72 Å, b = 210.72 Å, c = 324.41 Å. The structure was solved by molecular replacement, using the software MOLREP.[23] The unit cell size of the trigonal crystals strongly indicated that an entire ferritin molecule (24 subunits) was present in the asymmetric unit. A rough packing model was obtained by treating each single molecule as a featureless spherical object with a radius of ≈130 Å. An entire 24-mer of frog M ferritin was used as searching model (Protein Data Bank, PDB, code 1MFR) for the rotation and translation functions[24] after excluding nonprotein atoms and water molecules. The positions of the iron ions were determined from anomalous difference Fourier maps calculated using the program FFT (fast Fourier transform) from the CCP4 suite.[22] The anomalous signals corresponding to Fe were between 3.5 and 10.0 σ in the anomalous difference maps.

The structure was refined with the program REFMAC.[22,25] The refinement protocol involved a sequence of iterative manual rebuilding of the model and maximum-likelihood refinement.

The molecular graphics software Coot[26] was used to visualize the structures and for manual rebuilding and modeling of the missing atoms into the electron density. Water molecules were added using the program ARP/wARP.[27] The final model has been inspected manually and checked with the programs Coot[26] and PROCHECK.[28] The final model has good stereochemistry with 97.2% of residues in the favored regions and 2.8% in the additionally allowed and none in the disallowed regions of the Ramachandran plot.

A complete anomalous diffraction data set was collected on the iron-loaded frog M ferritin crystal type 2 at the ESRF beamline ID29 at the Fe−K edge (λ = 1. 7389 Å, T = 100 K). Images were collected on a PILATUS 6 M detector. Data reduction and structure solution were performed using the same procedures described above. The crystal belongs to the trigonal space group $P3_121$ with cell parameters a = 210.74 Å, b = 210.74 Å, c = 322.04 Å and with a whole frog M ferritin 24-mer in the asymmetric unit. The positions of the iron ions were determined from anomalous difference Fourier maps and the anomalous signals corresponding to Fe were between 5.0 and 10.5 σ. The structure was refined with the program PHENIX[29] using a protocol similar to that described above. The final model has good stereochemistry with 97.2% of residues in the favored regions and 2.8% in the additionally allowed and none in the disallowed regions of the Ramachandran plot.

A complete anomalous data set on the Cu-loaded frog M ferritin was collected at the ESRF on beamline ID29 at the Cu−K edge wavelength (λ = 1.378 Å, T = 100 K). Images were collected on a PILATUS 6 M detector. Data reduction has been performed as above. Copper-loaded frog M ferritin belongs to the trigonal space group $P3_121$ with cell parameters a = 210.21 Å, b = 210.21 Å, c = 322.80 Å and with a whole frog M ferritin 24-mer in the asymmetric unit. The structure was solved by molecular replacement, similarly to the previous structures. The positions of the copper ions were determined from anomalous difference Fourier maps. The anomalous signals corresponding to Cu ions were between 5.5 and 11.0 σ in the anomalous maps. The structure was refined with the program REFMAC[22,25] and validated by the same protocol used for Fe crystal 1. The final model has good stereochemistry with 96.9% of residues in the favored regions and 3.1% in the additionally allowed and none in the disallowed regions of the Ramachandran plot.

All the figures were generated using CCP4MG.[30]

The crystal form used for diffraction experiments contains one whole frog M ferritin molecule per asymmetric unit giving 24 independent copies of each subunit. This allowed us to obtain the standard deviations estimates (esd) of the differences in distances within the 24 subunits. The esd on Fe−Fe (Fe crystal 1) and on Cu−Cu distances obtained in this way is 0.1 and 0.4 Å, respectively. The estimated average error on the coordinates from crystallographic refinement is 0.2 Å for the iron adduct (Fe crystal 1), 0.4 Å for the second iron adduct (Fe crystal 2), and 0.2 Å for the copper adduct.[29,31] However, the actual error on the atomic positions of the metal ions is lower, although difficult to estimate, due to the larger electron density present on such centers.

The occupancies of almost all metal sites are fractional. In the case of the Fe crystal 1 and the Cu crystal, occupancies have been adjusted to obtain atomic displacement parameters (ADP) comparable with the surrounding protein atoms. The metal occupancies in the ferroxidase site have been fixed between 0.6 and 0.9 in Fe crystal 1 (average 0.8) and between 0.5 and 0.9 for the Cu crystal (average 0.6). For the second iron crystal, occupancies have been fixed to unity, and the ADP has been left to refine freely with values being at maximum 90% higher than the nearby atoms.

PDB Codes. Final coordinates and structure factors have been deposited in PDB under the accession code 3RBC for Fe crystal 1, 3RGD for Fe crystal 2, 3RE7 for the Cu crystal.

Electronic Absorption and Circular Dichroism Spectra. Absorption and circular dichroism spectra (300−850 nm) of frog M ferritin solutions were recorded under aerobic condition on a Varian Cary 50 Scan. The demineralized protein was titrated at first with 4 equiv of copper(II) ions (solution of $CuSO_4 \cdot 5\ H_2O$). The solution became light green with an electronic absorption spectrum having a very broad band centered at 740 nm. Then, 2 equiv of iron(II) ($FeSO_4 \cdot 7H_2O$ in HCl 0.1%) were added to this solution that immediately became dark gray and after 15 h turned orange, showing slow iron oxidation in the presence of copper.

Visible absorption spectra (300−850 nm) of the iron loaded crystals (Fe crystal 1) and copper loaded crystals were recorded on a GE Healthcare NanoVuePlus spectrophotometer and showed the same bands observed for the corresponding solutions.

RESULTS AND DISCUSSION

Iron(III) at the Ferroxidase Site. At variance with the already available structures, where the asymmetric unit was constituted by a single subunit and the 24-mer was generated by symmetry transformations, in all our crystals the asymmetric unit is constituted by the 24-mer, and data are independently obtained for the 24 subunits. They are identical within the experimental error (pairwise root-mean-square deviation, rmsd, values in the 0.21−0.26 Å). The structure of the polypeptide part is superimposable with that of the already available frog M ferritins (rmds values in the range 0.12−0.22 Å).

Crystals soaked for 90 min in iron(II) were rust orange and showed electronic absorption spectra typical for iron(III) ferritin in solution (see Experimental Procedures, Fe crystal 1).

dx.doi.org/10.1021/ja210084n | J. Am. Chem. Soc. 2012, 134, 6169−6176

Scheme 1. Proposed Structural Changes at the Ferroxidase Site upon Iron Oxidation[a]

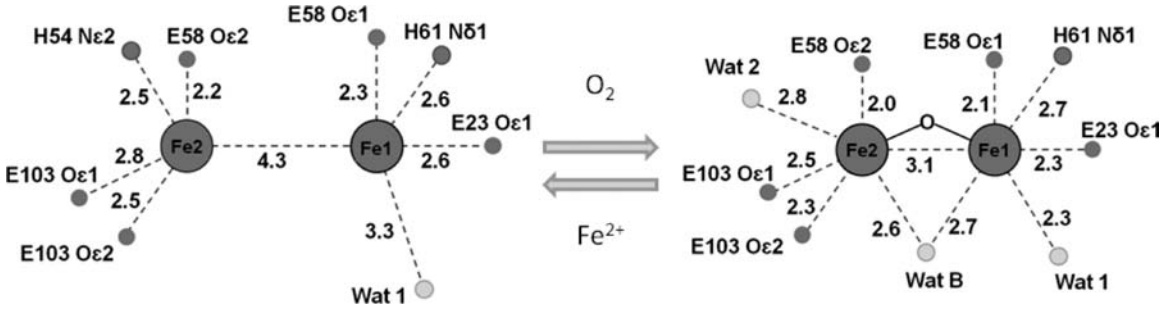

[a]The structural model for the iron(II) form (left panel) is based on the structure of the copper(II) derivative and supported by iron in crystal 2. Observed bonds are represented as broken lines, and their average lengths are provided in Å. The proposed oxo-bridge in the diferric center (right panel) is indicated by continuous lines.

This shows that iron(II) undergoes oxidation under these conditions. Invariably two iron ions in the ferroxidase site were detected with the same coordination environment and intermetal distances. Iron(III) at site 1 (Fe1) is coordinated to three protein residues (monodentate Glu23 on helix H1, Glu58, which bridges the two iron ions and His61 on helix H2), whereas iron(III) at site 2 (Fe2) binds only two protein residues (bridging Glu58 on helix H2 and Glu103 on helix H3 which acts as a bidentate ligand for Fe2) (Scheme 1, right panel, and Figure 2a). This coordination environment is consistent with previous nuclear magnetic resonance (NMR) data, where paramagnetic induced line broadening settled the position of dimeric iron(III) products away from helix H4, toward helices H1 and H2.[3] The B factors are essentially the same for Fe1 and Fe2. The refined occupancies for Fe1 and Fe2 are also the same within the experimental error and of the order of 80%. All coordination bonds, determined with a precision of 0.3 Å, are relatively long (Table S2, Supporting Information and Scheme 1, right panel). This effect may be, at least in part, attributable to the partial occupancy of the metal sites. Ligand−metal−ligand bond angles involving protein residues are provided in Table S3, Supporting Information. Fe1 and Fe2 structurally correspond to site A and B of *P. furiosus* (Figure S1C, Supporting Information), respectively, but the Fe−Fe distance observed in the 24 structurally independent subunits shows a much narrower spread with respect to the *P. furiosus* ferritin, being 3.1 ± 0.1 Å (Table S2, Supporting Information). Such a distance suggests the presence of an oxo/hydroxo bridge,[32,33] although not visible at the present resolution. Indeed, the expected short bonds for Fe(III)-oxo (≈1.80 Å)[32,34] hide the oxygen atom within the electron density of the di-iron cluster. The same intermetal distance, within experimental error, has been reported for the diferric product of ferritin catalysis from rapid freeze quench extended X-ray absorption fine structure measurements.[9] In the present structure, a further bridging water or hydroxo group is detectable at about 2.6 Å from each iron ion. Other interactions with terminal water molecules at longer distances are also operative (Table S2, Supporting Information); a caveat should be given that the position and number of water molecules around iron ions could be severely biased by the resolution limit and Fourier series truncation effects. As a whole, the Fe−Fe moiety with its nonprotein ligands is loosely anchored to the protein; Fe2 forms coordination bonds with two amino acids while Fe1 with three. For comparison, in other di-iron proteins the number of iron protein monodentate ligands for each iron ion ranges between 3 and 5.[35−37] In *E .coli* bacterioferritin, four ligands per iron are found with a total of five donor atoms, as one Glu acts as bidentate.[14] As a consequence of its less restricted coordination, in ferritins the iron(III) dimers may be pushed easily out by incoming iron(II).

Bipositive Cations at the Ferroxidase Site. Unraveling the mechanism by which iron(III) is substituted by iron(II) is another challenge, as the former is expected to bind electron donors with higher affinity than the latter.[38] The choice of copper(II) as a model for iron(II) was guided by the consideration that it is a bivalent transition-metal ion not prone to oxidation. Furthermore, copper(II) has coordination properties that a posteriori resulted in a distribution inside the protein that is more easily interpretable than that found for other divalent cations.[4,24] Consequently the structure of the copper(II) adduct, obtained with the same experimental approach as for the iron form, (Figure 2b) is enlightening. Two copper ions are present at sites 1 and 2 of the ferroxidase site. The Cu−Cu distance in the catalytic site is 4.3 ± 0.4 Å. While the coordination environment of copper at site 1 (Cu1) is similar to that of Fe1, copper at site 2 (Cu2) is bound to a further protein residue, i.e., His54 on helix H2 (Figure 2b), that changes its conformation with respect to iron crystal 1, going from the distal position adopted in the iron crystal 1 and in the apoprotein (PDB id: 4DAS) to a proximal position. Glu58 side chain reorients but still bridges the two metal ions, whereas no electron density attributable to other bridging atoms is observed. The metal−donor distances, that have a precision of 0.3 Å, are still somewhat larger than usual coordination distances (Table S2, Supporting Information). The coordination bond lengths and angles (Table S3, Supporting Information) for all the other protein ligands remain the same, within the experimental error, as in the iron crystal 1. When considering the atoms of the side chains of metal ligands in iron crystal 1 and copper crystal, rmsd values larger than 1 Å are found only for the Oε2 of Glu58 (1.6 Å) and for the Cδ2, Nδ1, and Nε2 of His54 (1.4, 1.8, and 1.7 Å, respectively).

His54 binding to cobalt(II) has been observed in crystals of ferritin obtained by cocrystallization.[4] It can be hypothesized that the coordination of iron(II) at the catalytic site is similar to that of copper(II). The presence of a bridging carboxylate and the absence of bridging water/hydroxo are consistent with the weak antiferromagnetic coupling derived from magnetic circular dichroism data on the iron(II) species.[5]

The picture resulting from the copper-bound structure suggests that oxidation requires changes in the coordination environment of iron(II) at site 2 and parallel reduction in the metal−metal distance. This is supported by the structure

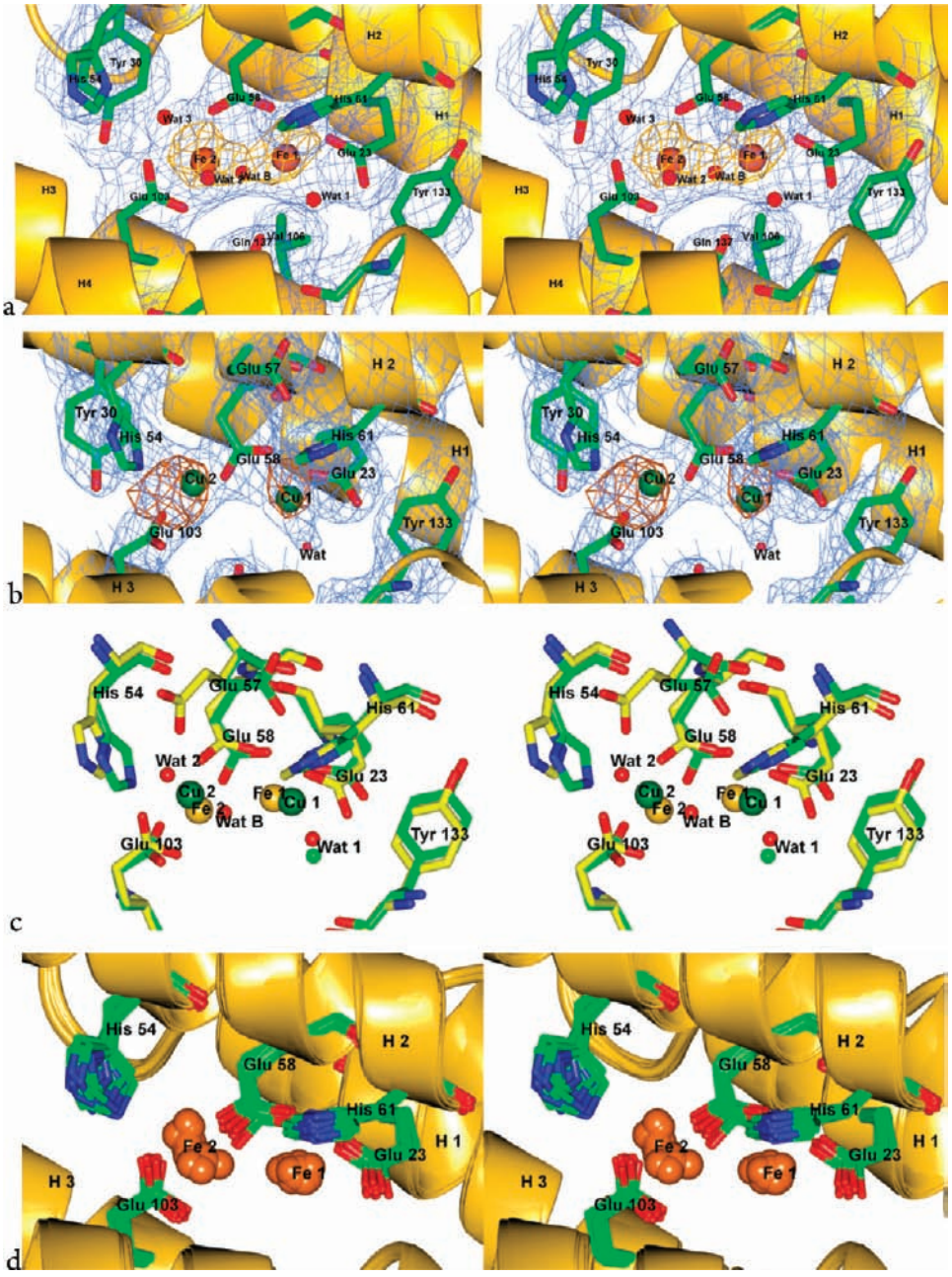

Figure 2. Stereo view of the coordination environment of iron(III) in (a) Fe crystal 1 and (b) copper(II) ions at the ferroxidase site; the models are superimposed to the 2Fo-Fc electron density map contoured at 1.0 and 1.5 σ, respectively, (blue wire) and to the anomalous difference electron density map contoured at 3.5 (yellow thick wire panel a) and 5.5 σ (copper thick wire panel b). (c) Least squares superimposition of the Fe bound (yellow sticks) and Cu bound (green sticks) ferritin. (d) Least squares superimposition of all 24 independent subunits of frog M ferritin Fe crystal 2. Iron ions at site 2 occupy two distinct positions, one similar to that of copper and one similar to that of iron in crystal 1. The same similarities hold for the side chain of His54. These findings suggest the rearrangement of the di-iron cluster upon oxidation.

obtained from the ferritin crystal soaked in $FeSO_4$ solution for a short time (1 min; see Experimental Procedures Section, Fe crystal 2). As shown in Figure 2d, the 24 independent ferritin subunits present in the crystal asymmetric unit show different structures of ferric dimers at the ferroxidase site, suggesting the presence of iron trapped in the initial docking site of the ferrous state and in the state corresponding to the final oxidation product. Although no direct evidence of the iron oxidation state in this crystal is available, besides the paler orange color with respect to Fe crystal 1, some structural data support this hypothesis. The shortest iron−iron distances correspond to that already observed in Fe crystal 1; the longest distances are suggestive of iron(II)−iron(II) sites[33,34] and compare very well with the copper(II)−copper(II) distance (Figure S2, Supporting Information). The same holds for Fe2−His54Nε2 distances. The shortest Fe2−His54 distances are found when the Fe1−Fe2 distances are the longest and vice versa, suggesting the involvement of His54 in iron(II) binding when it enters the ferroxidase site and its detachment from iron binding upon metal oxidation. At variance with crystal 1, the metal ion at site 2 has significantly larger B-factor than that at site 1, supporting the idea that the latter corresponds to a higher affinity preformed metal binding site. At site 2 affinity is modulated by the metal ion oxidation state.

dx.doi.org/10.1021/ja210084n | J. Am. Chem. Soc. 2012, 134, 6169−6176

The detachment of His54 in passing from iron(II) to iron(III) is due to the establishment of a short Fe(III)−Fe(III) distance characteristic of a μ-oxo-bound moiety. When iron oxidation occurs via dioxygen, the bridging oxygen atom forces iron at site 2 to move toward Fe1, breaking the Fe2−His54 bond; as a consequence, the His54 side chain reorients (Figure 2c) going from the proximal to the distal conformation. The new position of iron is outside the binding range for His54 (Figure 2c). His54 may assist an incoming iron(II) to replace iron(III). The structure of iron(III) (Scheme 1, right panel) therefore describes the situation of the transient iron(III) product at the catalytic site, while that of copper(II) may represent the prereactive conformation of iron(II) (Scheme 1, left panel). Copper(II), which does not react with oxygen, remains trapped in the prereactive conformation. Furthermore, the presence of copper(II) significantly slows down the iron oxidation reaction in competition binding experiments. This was demonstrated by adding 2 equiv of iron(II) at ferritin containing 4 equiv of copper(II) ions. Fifteen hours were needed before the solution turned into orange, i.e., before iron is oxidized (see Experimental Procedures Section).

Other Metal Binding Sites. The complete picture of ferritin provided by crystallography (Fe crystal 2 data) includes iron occupying the so-called C3 pore (Figure 3a). Distinct anomalous signals corresponding to iron ions are clearly detected, above noise, in the channel and attributed to monomeric iron species caught at different steps along the passage, at varying distances and occupancies from Glu130 side chains. The crystallographic data cannot reveal the iron oxidation state at the C3 pore, however, it is possible that the signals at the ternary axes arise from not yet reacted iron(II), which is attracted by internal negative charges in the channel, consistently with previous reports on other bivalent metal ions.[4] This observation supports the proposal that the C3 channel may represent the entry pore.

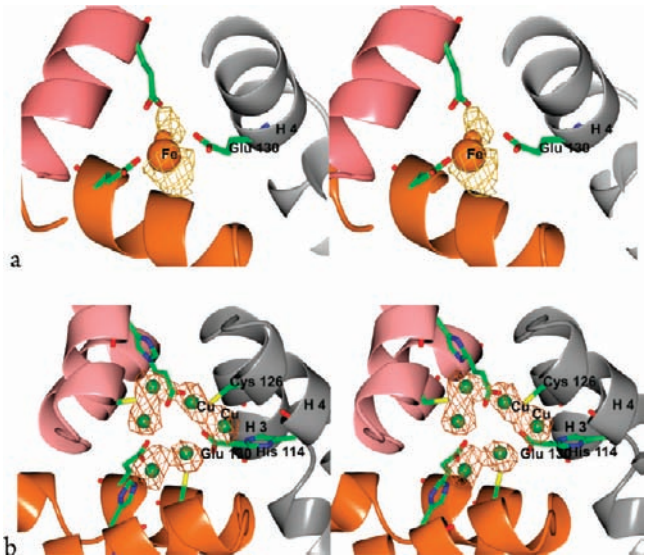

Figure 3. Stereo views of the structures for (a) Fe crystal 2 and (b) copper at the C3 pore. For iron, distinct anomalous signals (gold thick wire contoured at 3.5 σ) corresponding to different positions of iron ions are seen in the channel. The iron positions are represented as spheres whose diameter is proportional to the observed anomalous signal intensity. In the case of copper, a completely new setting is observed with three pairs of copper(II) ions bound to the three symmetry-related subunits(copper thick wire contoured at 5.5 σ).

A weak anomalous signal and a blob of electron density indicate the presence of iron ions also in the pores corresponding to the 4-fold axes (C4 pores), at a distance (3.0−3.2 Å) from the Nε2 of His169 that suggest weak or no coordination (Figure 4a). This single metal ion observed at the end of the C4 pore may diffuse there from the bulk solution rather than through the ferroxidase site and therefore may represent a nonphysiological situation. Indeed, the path from the catalytic site to the cavity was traced by NMR[3] that, together with other spectroscopies,[9,39−41] has shown that product migration proceeds via iron clusters.

Copper(II) at the C3 and C4 pores (Figures 3b and 4b) has arrangements different from iron and, presumably, not functionally relevant. For instance, the ternary axis hosts beautiful exanuclear copper clusters bound to His114 and Glu130 and to the Cys126 sulfur (of each subunit) that acts as bridging ligand to two adjacent copper ions. The Cys126 side chain rotates about 180° with respect to the unbound structure in order to bind copper (Figure 3b). At the quaternary axis, the four His169, at variance with Fe crystal 2, extend about 1.0 Å into the pore to bind the copper ion (Figure 4b).

CONCLUSIONS

The structure determinations of M ferritin crystals, obtained under aerobic conditions for two different soaking times in iron(II) solutions, reveal the binding of iron to a higher eukaryotic ferritin. The crystal form used in this study contains 24 independent subunits in the asymmetric unit, providing highly redundant comparisons between subunits. This situation, for long soaking times (Fe crystal 1), results in the observation of invariant diferric sites where the Fe−Fe average distance of 3.1 ± 0.1 Å is, within experimental error, the same found by X-ray absorption spectroscopy[9] and strongly indicates the presence of a μ-oxo/hydroxo bridge between the irons. Two copper(II) ions also bind at the ferroxidase site, giving rise to a dinuclear center with longer intermetal distances and with His54 as an extra ligand for the metal at site 2. This arrangement of the ligands is comparable, although not identical, to that reported for cobalt(II), where three ions were detected at the ferroxidase site;[4] while at site 1, a single cobalt ion is detected, and at site 2, two alternative positions for cobalt ions are observed, which correspond to His54 in two conformations (which we have called proximal and distal) (Figure S2, Supporting Information), but always acting as a metal ligand.

The redundant information for the 24 independent subunits allows the detection of two different types of di-iron centers in the crystal soaked for the shorter time (1 min, Fe crystal 2). The metal positions are, within the experimental error, the same as that of iron(III) in the Fe crystal 1 and copper(II)-containing crystals, as depicted in Scheme 1. The findings on Fe crystal 2, therefore, complete and support the mechanistic proposal of Scheme 1 and may provide a snapshot of the structural changes occurring upon iron oxidation.

The ferroxidase site of M frog ferritin, and site 2 in particular, appears to be quite flexible, depending on the oxidation state of the hosted metal ion. The frog M ferritin His54 is substituted by a Gln in *P. furiosus* (which shares an overall sequence identity of 32% with M frog ferritin) and by a Glu in *Pseudonitzschia multiseries* (overall identity of 27%). These differences in sequence translate into different metal binding

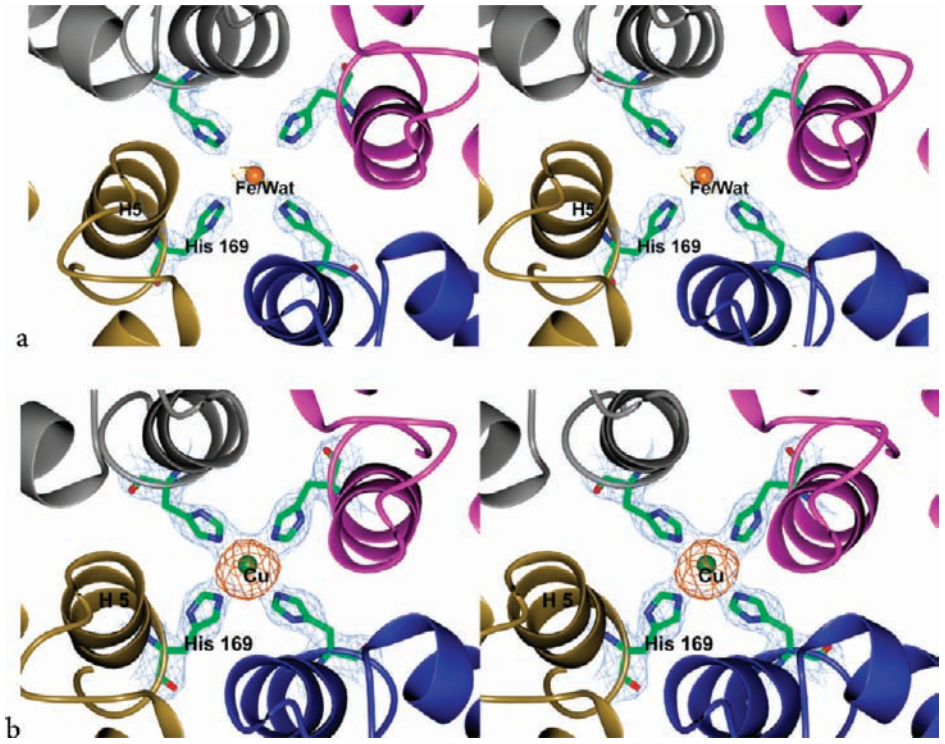

Figure 4. Top-down view (stereo mode) of the C4 pore: (a) an anomalous signal between is observed in all four-fold sites and can be interpreted as the presence of a Fe ion (gold thick wire). (b) In the case of copper (copper thick wire), the four His169 side chains move closer to the metal ion reaching proper coordination distances (2.2−2.5 Å); a water molecule (not shown) binds copper from the inner part of the channel, completing a square pyramidal coordination.

sites, as observed in the respective crystal structures (Figure S1, Supporting Information). A comparison of frog M ferritin, with the sequences of other hundreds of ferritins from eukaryotes having ≥66% sequence identity with it, shows that the position equivalent to His54 is generally occupied by Asn or Gln, which may play the same game as to provide flexible ligands to incoming divalent cations and guide the proposed shuttling mechanism.

The path from the catalytic site to the biomineralization cavity is traced only by NMR[3] because transient coordination sites along the path are poorly populated, as expected on functional grounds. The observation of iron at different positions within the three-fold pores suggests a possible pathway for iron entrance in the protein.

The comparison between the iron(III) and metal(II) derivatives suggests a detailed mechanism for the oxidation reaction in eukaryotic ferritins. Iron(II) is presumably attracted by electrostatic forces to the active site, where its binding (in a prereactive conformation) to site 2 is favored by His54. Oxidation and formation of diferric oxo/hydroxo bridges stabilizes the coordination cluster, imposing a shorter intermetal distance, and destabilizes the binding to the protein. New incoming iron(II) may push the di-iron(III) moiety toward the cavity.

■ ASSOCIATED CONTENT

Supporting Information

Tables reporting data collection and refinement statistics. (Table S1) and main structural features of the active site (Table S2). A figure comparing metal binding sites within the four-helix bundle channel of ferritin from different organisms (Figure S1). A figure (Figure S2) comparing the coordination environment of various metal ions bound to M frog ferritin. This material is available free of charge via the Internet at http://pubs.acs.org.

■ AUTHOR INFORMATION

Corresponding Author

ivanobertini@cerm.unifi.it

Notes

The authors declare no competing financial interest.

■ ACKNOWLEDGMENTS

We thank Marta Argenti for preliminary spectroscopic characterization of copper ferritin and Manuela Benvenuti for help in protein crystallization experiments. S.M. and C.P. acknowledge the financial support from CIRMMP. We acknowledge ESRF (Grenoble) for having provided access to the ID14-4 and ID29 beamlines. The research was funded by Italian MIUR (contract FIRB PROTEOMICA MIUR -RBRN07BMCT) and by the NIH (grant DK20251).

■ REFERENCES

(1) Liu, X.; Theil, E. C. *Acc. Chem. Res.* **2005**, *38*, 167−175.
(2) Theil, E. C. *Curr. Opin. Chem. Biol.* **2011**, *15*, 1−8.
(3) Turano, P.; Lalli, D.; Felli, I. C.; Theil, E. C.; Bertini, I. *Proc. Natl. Acad. Sci. U.S.A.* **2010**, *107*, 545−550.
(4) Tosha, T.; Ng, H.-L.; Bhattasali, O.; Alber, T.; Theil, E. C. *J. Am. Chem. Soc.* **2010**, *132*, 14562−14569.
(5) Schwartz, J. K.; Liu, X. S.; Tosha, T.; Theil, E. C.; Solomon, E. I. *J. Am. Chem. Soc.* **2008**, *130*, 9441−9450.
(6) Bou-Abdallah, F.; Zhao, G.; Mayne, H. R.; Arosio, P.; Chasteen, N. D. *J. Am. Chem. Soc.* **2005**, *127*, 3885−3893.
(7) Zhao, G.; Bou-Abdallah, F.; Arosio, P.; Levi, S.; Janus Chandler, C.; Chasteen, N. D. *Biochemistry* **2003**, *42*, 3142−3150.

(8) Bou-Abdallah, F.; Arosio, P.; Santambrogio, P.; Yang, X.; Janus Chandler, C.; Chasteen, N. D. *Biochemistry* **2002**, *41*, 11184−11191.
(9) Hwang, J.; Krebs, C.; Huynh, B. H.; Edmondson, D. E.; Theil, E. C.; Penner-Hahn, J. E. *Science* **2000**, *287*, 122−125.
(10) Tatur, J.; Hagedoorn, P. L.; Overeijnder, M. L.; Hagen, W. R. *Extremophiles* **2006**, *10*, 139−148.
(11) Tatur, J.; Hagen, W. R.; Matias, P. M. *J. Biol. Inorg. Chem.* **2007**, *12*, 615−630.
(12) Marchetti, A.; Parker, M. S.; Moccia, L. P.; Lin, E. O.; Arrieta, A. L.; Ribalet, F.; Murphy, M. E.; Maldonado, M. T.; Armbrust, E. V. *Nature* **2009**, *457*, 467−470.
(13) Carrondo, M. A. *EMBO J.* **2003**, *22*, 1959−1968.
(14) Crow, A.; Lawson, T. L.; Lewin, A.; Moore, G. R.; Le Brun, N. E. *J. Am. Chem. Soc.* **2009**, *131*, 6808−6813.
(15) Weeratunga, S. K.; Lovell, S.; Yao, H.; Battaille, K. P.; Fischer, C. J.; Casey, E. G.; Rivera, M. *Biochemistry* **2010**, *49*, 1160−1175.
(16) Nordlund, P.; Sjöberg, B.-M.; Ecklund, H. *Nature* **1990**, *345*, 593−598.
(17) Rosenzweig, A. C.; Brandstetter, H.; Whittington, D. A.; Nordlund, P.; Lippard, S. J.; Frederick, C. A. *Proteins* **1997**, *29*, 141−152.
(18) Cho, K. J.; Shin, H. J.; Lee, J. H.; Kim, K. J.; Park, S. S.; Lee, Y.; Lee, C.; Park, S. S.; Kim, K. H. *J. Mol. Biol.* **2009**, *390*, 83−98.
(19) Hamburger, A. E.; West, A. P.; Hamburger, Z. A.; Hamburger, P.; Bjorkman, P. J. *J. Mol. Biol.* **2005**, *10*, 558−569.
(20) Leslie, A. G. W. *Acta Crystallogr., Sect. D: Biol. Crystallogr.* **2006**, *62*, 48−57.
(21) Evans, P. R. *Joint CCP4 and ESF-EACBM Newsletter* **1997**, *33*, 22−24.
(22) Collaborative Computational Project, Number 4. *Acta Crystallogr., Sect. D: Biol. Crystallogr.* **1994**, *D50*, 760−763.
(23) Vagin, A. A.; Teplyakov, A. *J. Appl. Crystallogr.* **1997**, *30*, 1022−1025.
(24) Ha, Y.; Shi, D.; Small, G. W.; Theil, E. C.; Allewell, N. M. *J. Biol. Inorg. Chem.* **1999**, *4*, 243−256.
(25) Murshudov, G. N.; Vagin, A. A.; Dodson, E. *Acta Crystallogr., Sect. D: Biol. Crystallogr.* **1997**, *53*, 240−255.
(26) Emsley, P.; Cowtan, K. *Acta Crystallogr., Sect. D: Biol. Crystallogr.* **2004**, *60*, 2126−2132.
(27) Perrakis, A.; Morris, R. J. H.; Lamzin, V. S. *Nat. Struct. Biol.* **1999**, *6*, 458−463.
(28) Laskowski, R. A.; MacArthur, M. W.; Moss, D. S.; Thornton, J. M. *J. Appl. Crystallogr.* **1993**, *26*, 283−291.
(29) Adams, P. D.; Afonine, P. V.; Bunkòczi, G.; Chen, V. B.; Davis, I. W.; Echols, N.; Headd, J. J.; Hung, L.-W.; Kapral, G. J.; Grosse-Kunstleve, R. W.; McCoy, A. J.; Moriarty, N. W.; Oeffner, R.; Read, R. J.; Richardson, D. C.; Richardson, J. S.; Terwilliger, T. C.; Zwart, P. H. *Acta Crystallogr., Sect. D: Biol. Crystallogr.* **2010**, *66*, 213−221.
(30) Potterton, L.; McNicholas, S.; Krissinel, E.; Gruber, J.; Cowtan, K.; Emsley, P.; Murshudov, G. N.; Cohen, S.; Perrakis, A.; Noble, M. *Acta Crystallogr., Sect. D: Biol. Crystallogr.* **2004**, *60*, 2288−2294.
(31) Murshudov, G. N.; Vagin, A. A.; Dodson, E. J.; Acta Crystallogr, D *Acta Crystallogr., Sect. D: Biol. Crystallogr.* **1997**, *1*, 240−255.
(32) Vincent, J. B.; Olivier-Lilley, G. L.; Averill, B. A. *Chem. Rev.* **1990**, *90*, 1447−1467.
(33) Tshuva, E. Y.; Lippard, S. J. *Chem. Rev.* **2004**, *104*, 987−1012.
(34) Kurtz, D. M. Jr. *Chem. Rev.* **1990**, *90*, 585−606.
(35) Strand, K. R.; Karlsen, S.; Kolberg, M.; Rohr, A. K.; Gorbitz, C. H.; Andersson, K. K. *J. Biol. Chem.* **2004**, *279*, 46794−46801.
(36) Rosenzweig, A. C.; Frederick, C. A.; Lippard, S. J.; Nordlund, P. *Nature* **1993**, *366*, 537−543.
(37) Holmes, M. A.; Trong, I. L.; Turley, S.; Sieker, L. C.; Stenkamp, R. E. *J. Mol. Biol.* **1991**, *218*, 583−593.
(38) Do, L. H.; Lippard, S. J. *J. Am. Chem. Soc.* **2011**, *133*, 10568−10581.
(39) Bou-Abdallah, F.; Papaefthymiou, G. C.; Scheswohl, D. M.; Stanga, S. D.; Arosio, P.; Chasteen, N. D. *Biochem. J.* **2002**, *364*, 57−63.
(40) Treffry, A.; Bauminger, E. R.; Hechel, D.; Hodson, N. W.; Nowik, I.; Yewdall, S. J.; Harrison, P. M. *Biochem. J.* **1993**, *296*, 721−728.
(41) Jameson, G. N.; Jin, W.; Krebs, C.; Perreira, A. S.; Tavares, P.; Liu, X.; Theil, E. C.; Huynh, B. H. *Biochemistry* **2002**, *41*, 13435−13443.